5-2017

Renewable and Abundant Battery Components

Jordan T. Sutton
University of Tennessee, Knoxville, jsutto16@vols.utk.edu

Daniel San Roman
University of Tennessee, Knoxville

Austin Thomas
University of Tennessee, Knoxville

Daniel Kitsmiller
University of Tennessee, Knoxville

Alec Affolter
University of Tennessee, Knoxville

Renewable and Abundant Battery Components

Alec Affolter, Daniel Kitsmiller, Daniel San Roman, Jordan Sutton, Austin Thomas
Material Science and Engineering Department, University of Tennessee

I. ABSTRACT

Lithium electrochemical cells have high specific energy capacities with long cycling capabilities, making them a promising choice to solve energy storage problems in electric vehicles and variable generation sources. Graphite, a conductive carbon structure, is commonly used as a battery anode material that stores lithium ions within its layers. Renewable lignin-based carbon composites potentially offer a sustainable and cost-effective alternative to mined graphite. This project builds on previous research on lignin, a carbon-saturated, polymer waste product from wood pulping, that can be converted to a graphitic carbon composite. The lignin must undergo a process called carbonization in which organic molecules are burned-off leaving graphite particles and amorphous carbon regions. In this investigation, the humidity in the atmosphere during heat treatments was varied to determine its effect on the resulting microstructure. SEM imaging of the post-pyrolyzed samples showed a change in the porous structure potentially resulting from increased lignin monomer mobility. X-ray diffraction determined that crystallite size of graphite nanoparticles after carbonization is negatively correlated with humidity. SEM and XRD analysis were also used to identify the weight percent of iron, sulfur, and sodium contaminants introduced during processing.

II. INTRODUCTION

Battery companies desire products made from inexpensive and sustainable sources. Dr. David Harper at the Center for Renewable Carbon (CRC) is conducting research on replacing the flake graphite commonly used in Li-ion battery anodes with a carbon composite material made

from lignin. Lignin is one of the main components of wood pulp and is therefore a high-volume waste product of the Kraft pulping process used in the paper industry. Currently, most of this waste is burned as it has little monetary value and is not worth the overhead costs of marketing [1]. That can change, however, if the lignin in this waste can be used as a viable precursor material for high carbon content char that can be used as a substitute in conventional flake graphite, activated carbon, and carbon black processes. The method by which lignin is transformed into a carbon composite is through heat treating the lignin in a three step process known as carbonization. The lignin undergoes two heating cycles, and is ball milled between the two heating cycles. Stabilization and pyrolysis occur during the first heating cycle, followed by a reduction step in the second heating cycle. Stabilization is a conditioning step to provide the material with a temperature resistant structure necessary to withstand high temperatures during the pyrolysis and reduction steps. Pyrolysis is the decomposition of organic material exposed to high temperatures in an oxygen-free environment. The reduction step is performed in order to rid the lignin of any remaining oxygen that is attached to the structure and introduce hydrogen for stability. After undergoing both heating cycles, the carbon composite material is fabricated into coin cell batteries for testing at Oak Ridge National Lab (ORNL). The goal of this investigation is to improve the process by controlling the amount of humidity fed into the furnace during the first heating cycle and determining its effect of the material structure.

II.A. Material Selection

Lithium electrochemical cells have high specific energy capacities with long cycling capabilities; as these battery prices continue to fall, they remain a top choice for future energy storage [2]. Batteries must achieve high energy storage capacities while maintaining reasonable

current densities and lifetimes. Batteries must also be safe for consumers, reliable for emergency situations and military personnel, and nontoxic for the environment upon disposal. All of these constraints make material selection essential when fabricating modern batteries. When considering the anode material for lithium ion batteries, there are a variety of choices. The most common choice for the active material in anodes is graphite. Graphite is a crystalline solid with a black/grey color and a metallic sheen. Due to its electronic structure, it is highly conductive and can reach 25,000 S/cm^2 in the plane of a single-crystal [3]. Graphite is commonly used as the active material in negative electrodes because it can reversibly place lithium ions between graphene layers, a process known as intercalation. Figure 1 shows how the Li ions fit into the anode and cathode structure.

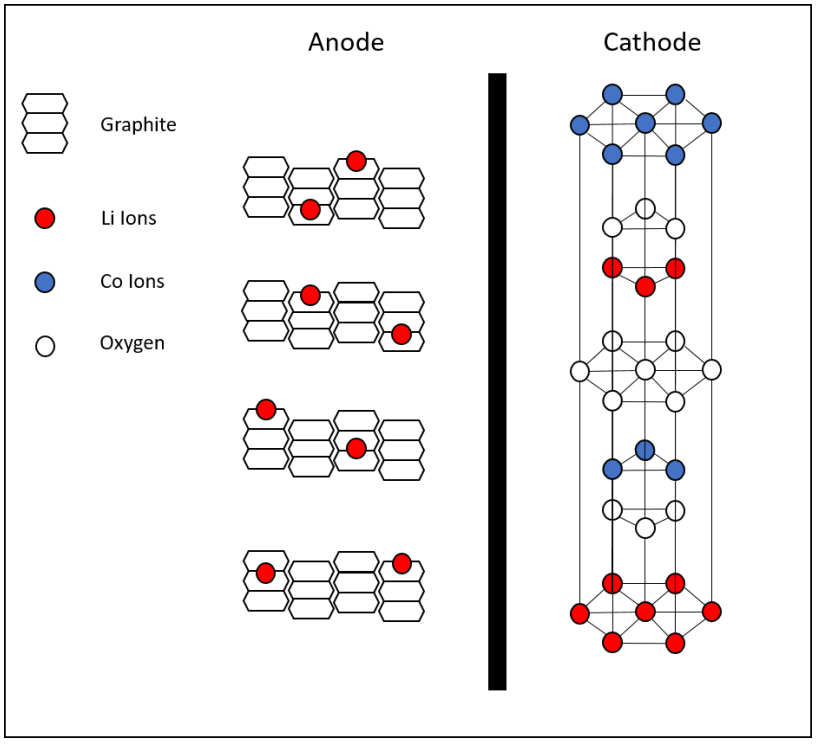

Figure 1- *Li-Ion anode/cathode. Lithium ions (red) diffuse into the graphite matrix during the charging sequence. They are stored in a ratio of 1 Li ion for every 6 carbon atoms*

This reversible electrochemical capability is maintained over several of thousands of cycles in batteries with optimized electrodes. Graphite used in batteries comes mainly from mining graphite ore [4]. There are disadvantages to graphite that include cost, sustainability, environmental impact, and national security. This paper investigates lignin biomass material as a replacement battery anode material for lithium ion batteries and explains current research on improving lignin structure to achieve desirable properties and overall battery performance.

The carbon composite structure that the lignin powder is processed into has been found to interact with lithium ions in a manner different than the typical Li-C_6 intercalation that is seen in Figure 1. Instead of the lithium ions settling between the layers of graphitic crystals, they tend to settle on the edges of the graphitic nanoparticles that form in the structure. This interaction is modeled in Figure 2.

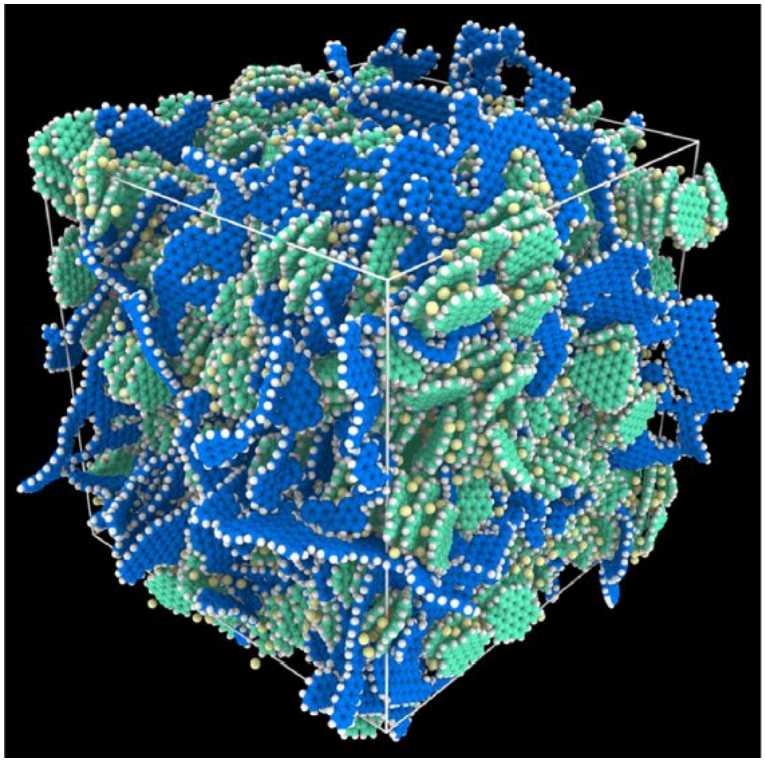

Figure 2 - *Model of the carbon composite structure after reduction. The structure consists of amorphous carbon (blue), graphitic nanoparticles (green), hydrogen (white) and lithium ions (yellow) [5]*

II.B. Source of Lignin

The Kraft pulping process is used in over 80% of the chemical pulp produced in the US and currently is the dominant wood pulping process around the world [6]. The Kraft process turns wood into wood pulp by treating wood chips with a combination of hot water, sodium hydroxide, and sodium sulfide, and then submitting the chips to several chemical and mechanical cycles. The byproducts of the Kraft process are various effluent gases and a dark liquid commonly referred to as 'black liquor', which contains 3.5 to 5% lignin by weight from the wood chips [6]. One of the advantages of the Kraft process is that they make use of a 'recovery boiler', in which they burn the black liquor as a source of fuel for the rest of the plant. This allows the plant to recover and reuse many inorganic chemicals as well as produce much of their own energy needs; this aids in lowering the operation costs of Kraft pulp plants. While the use of the black liquor as a fuel source is a benefit to the plants, it is being used in this way because its component materials, specifically the organic materials, have little or no economic value outside of this use. The paper mill industry is interested in monetizing the material beyond an overhead cost reduction. If the lignin present in this waste product could successfully be used as a precursor carbon source material, the price of the raw lignin would increase substantially, and these manufacturing plants would have to option to sell the process by-product for a profit.

Over 100 million tons of lignin per year are produced during the pulping process [7]. The price of lignin only reaches $0.04/kg as fuel for the pulp mill, so papermaking companies view this as an area with a high potential for additional profit [8]. As the proliferation of mobile electronic devices continues, the demand for inexpensive, high capacity batteries will continue to rise. Lignin is posed as a promising option to meet that demand as it is inexpensive and

abundant. The anode in a battery currently represents 14-15% of the total cost of a battery [9]. By using the carbon composite instead of battery grade flake graphite, which costs $15/kg, the price of the battery can be lowered significantly [7].

II.C. Background on Lignin

Lignin, cellulose, and hemicellulose are the three major components in the structure of plant cell walls. Lignin is the phenolic resin that binds the fibers in wood together [10]. In the Kraft process, wood is chemically treated to break the bonds between lignin, hemicellulose, and cellulose, producing the black liquor that contains the majority of the lignin from the wood. This lignin consists of three major constituents, called *p*-hydroxyphenyl (H), guaiacyl (G), and syringyl (S) [11]. Lignin from tree species has a varying structure with differing combinations of H, G, and S, as well as amorphous components. These units are shown below in Figure 3.

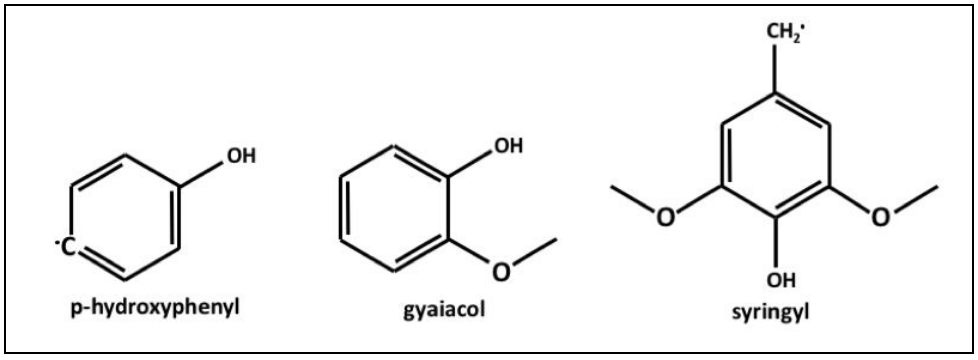

Figure 3 - *Three major components of lignin (H, G, S).*

Previous work has investigated pyrolysis and carbonization of hardwood lignin-based carbon fibers (LCF) for utilization as anodes in coin cell batteries [12]. These LCF anodes were shown to produce specific charge capacities comparatively close to that of traditional graphitic anodes found in lithium-ion batteries. This work presents the findings of LCFs from hardwood trees used in the Kraft pulping process. The woods used in pulping processes can be classified into two categories: hardwoods and softwoods. Hardwood deciduous trees include oak, hickory,

and maple. These trees lose their leaves in the fall and grow at a much slower rate than softwoods. Their slow growth reflects the shorter wood fibers that give them their high density, as shown below in Figure 4. Conifer trees, such as pine or cedar, generally are softwoods. They are typically evergreen and grow at a much faster rate, making them attractive for the paper industry. Furthermore, their longer wood fibers are beneficial towards keeping paper held together, and these benefits result in softwoods being more utilized in the paper industry than hardwoods. Because of this, the softwood lignin byproduct produced from the Kraft process, called Kraft softwood lignin (KSL), is much more abundant than the byproduct lignin from hardwoods. In addition, softwoods generally contain more lignin, at 25-35%, than hardwoods, at 20-25% [12]. Previous work highlights a paramount discovery—that a renewable, abundant, and economical method for creating the anodes in traditional batteries exists, and it competitively challenges traditional anode materials [13]. Although, the use of KSL shows more promising results, as it is more readily available and abundant than lignin produced from hardwoods.

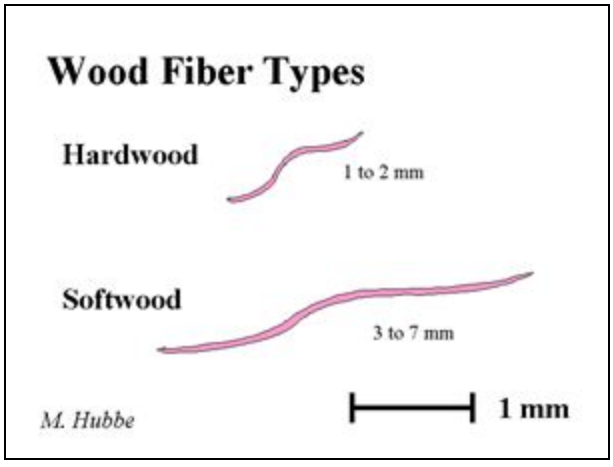

Figure 4 - *Range of hardwood and softwood fiber length. The prevalent extension of the fibers in the softwoods is what makes softwoods appealing to paper milling companies [9].*

II.D. Graphite Considerations

Flake graphite is the most commonly used component for anodes due to its cheap cost and its effective performance as battery anodes. One of the political and economic disadvantages to using flake graphite, however, is that China controls 70% of the world's graphite supply [5]. Due to their dominance in the graphite industry, global markets are reliant on China to provide for the rising demand in graphite. The United States does not have access to a competitive substitute. If the relationship between the United States and China ever became severely strained China would have full control over a valuable resource used in modern society. With this in mind it becomes clear that possible alternatives to flake graphite are of interest to the United States to reduce reliability on China's resources.

Although flake graphite is an inexpensive and effective resource for battery anodes, the mining of graphite is an environmentally unfriendly process that causes pollution in the nearby area [14]. The wells of neighboring villages become polluted and undrinkable while also causing damage to the crops. The graphite can even be visible in the air around them and build up in the homes of the villagers, causing health complications as the powder is inhaled. If lignin could be used to make a carbon composite substitute for flake graphite the environmental damage could be significantly reduced. Additionally, flake graphite is not a renewable resource and will eventually become depleted. Finding an alternative renewable resource like carbon composites from lignin would be an important step in preventing the loss of an important resource in modern society. Lignin carbon composites could also be a viable alternative to other materials such as carbon black and activated carbon by varying the carbonization process.

III. METHOD

III.A. Constructing the Manifold

For our research plan, the group designed a manifold that would allow for gas flow and humidity control, as seen in Figure 5. From the compressed cylinder, the inert gas flows through a regulator and splits into two paths. One path bubbles the gas through water, introducing water vapor to the stream. The dry air stream is regulated by a mass flow controller (Cole Parmer MC Series), and the two streams mix back together. This configuration allows for the control of the humidity by changing the proportion of dry and wet gas that are mixed together. A dew point transmitter (Michell Instruments SF52) reads the dew point temperature of the inlet gas before it enters the furnace.

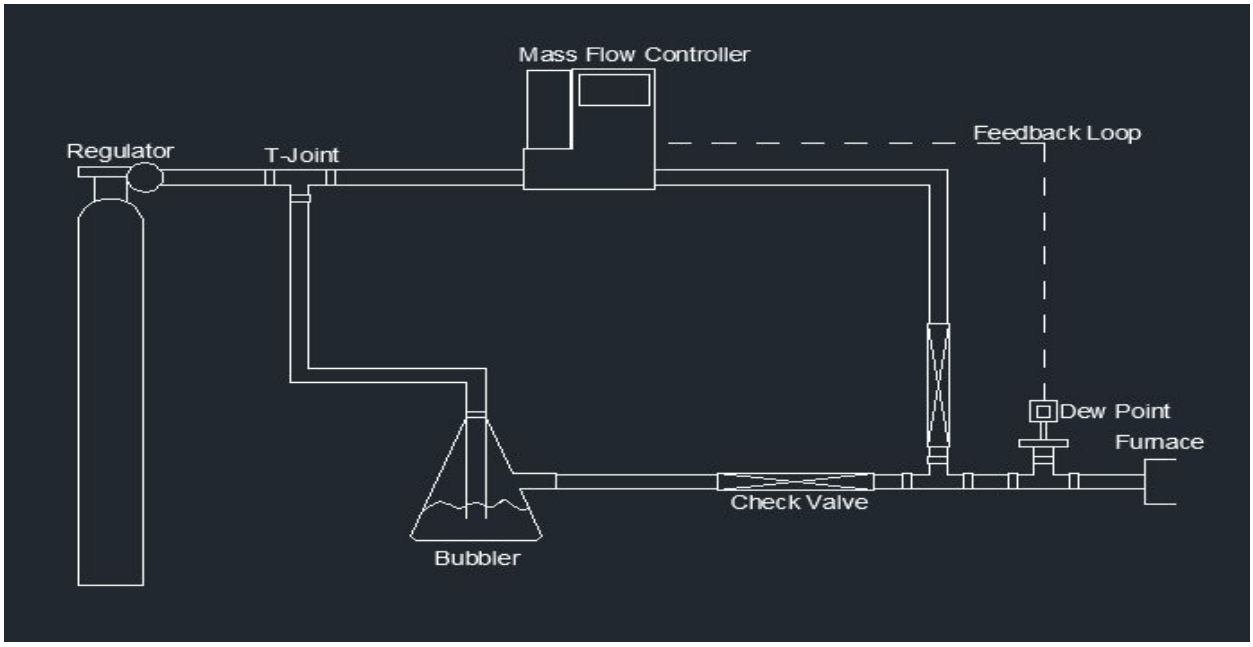

Figure 5 - *Diagram of the prototype gas manifold to be implemented in this experiment. This design offers humidity control, and the possibility of a humidity profile for later testing.*

To understand the dew point measurements, it was necessary to use the August-Roche-Magnus approximation with logged data for the air and dew point temperatures to determine the relative humidity [15]. From the relative humidity of the gas at a given temperature, one can read a psychrometric chart to find the corresponding absolute humidity. This value is typically given by the mass of water divided by the volume of air. By studying psychrometric charts, the group realized that significant increases in water content of the inlet gas could be achieved by increasing the temperature of the inert gas and water in the bubbler. For comparison, at 100 % relative humidity, a temperature difference of 20 °C and 80 °C yields an absolute humidity of 0.017 and 0.291 kg/m3, respectively. Figure 6 gives a schematic of the energy and mass balance associated with the system. The heat leaving the system will determine the temperature of the gas and the allowable amount of water in the vapor phase. The heat leaving the system can be increased by applying heat to the bubbler or preheating the inlet gas.

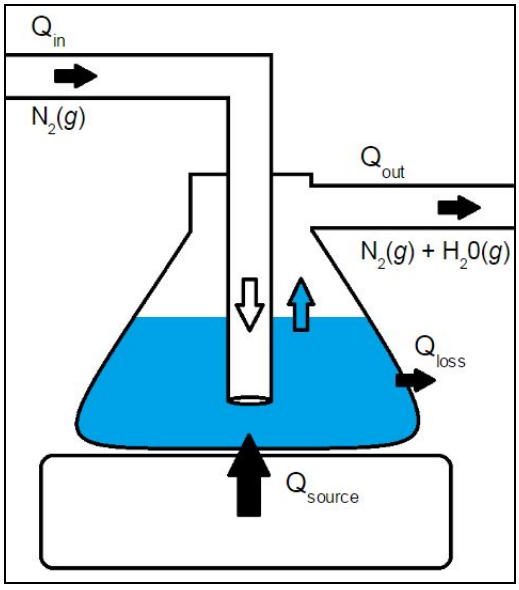

Figure 6 - *Energy and mass balance in the bubbler system. The heat leaving the system will determine the temperature of the gas and the allowable amount of water in the vapor phase.*

Construction of the manifold began with the mass flow controller (MFC) and the dew point transmitter. For flexibility, polymer tubing was utilized for most of the prototype manifold. A glass flask was used as a temporary bubbler on the wet line. The dew point transmitter requires a DC power supply between 8-24 Volts and gives a 4-20 mA signal. This signal is read by a multimeter and can be interpolated to a dew point temperature range of -40 to +60 °C.

A number of significant changes were made to the manifold over the course of the experiment. The first was that all of the polymer tubing from the in-line heater to the furnace was replaced with stainless steel tubing. It was believed that the polymer tubing would degrade during the heating of the gas. Having the stainless steel tubing also allows for the manifold to be more rigid as a whole. The glass bubbler was replaced with a custom-made stainless steel bubbler that integrated into the metal tubing. This bubbler was designed as a hollow tube, with the inlet tube extending down inside the main vessel so that the incoming gas would bubble up through the water in the vessel. It was positioned in the manifold beneath the main line, and the outlet tube was angled up so that any condensation formed in the tube would flow back into the bubbler. The top was fixed with a removable screw to allow water to be poured in.

The nitrogen gas was heated at two locations within the manifold. First, the inlet gas was heated by an in-line heater placed before the junction where the gas split between the wet and dry lines. The water in the bubbler was also heated using heating tape, which was wound from the bottom of the bubbler to halfway up its sides. The stainless steel tube containing water-saturated gas was heated with heating tape after the wet and dry lines converged to prevent condensation. This heating tape was wound tightly around the pipes all the way from the bubbler outlet to the dew point transmitter.

Other significant changes made to the manifold were the addition of a flow meter at the beginning of the manifold, and a thermocouple added right after the dew point transmitter. The flow meter was added to allow for additional control of the input flow, as the mass flow meter only controlled the flow into the dry line. Controlling both were necessary in order to maintain a stable temperature and dew point at higher temperatures. The thermocouple was added so that the temperature of the inlet gas could be monitored in real time. Both the temperature of the gas and the dew point were monitored during processing, and changes were made to the flow and temperature in order to maintain a stable dew point during the runs. A schematic of the final manifold can be seen in Figure 7.

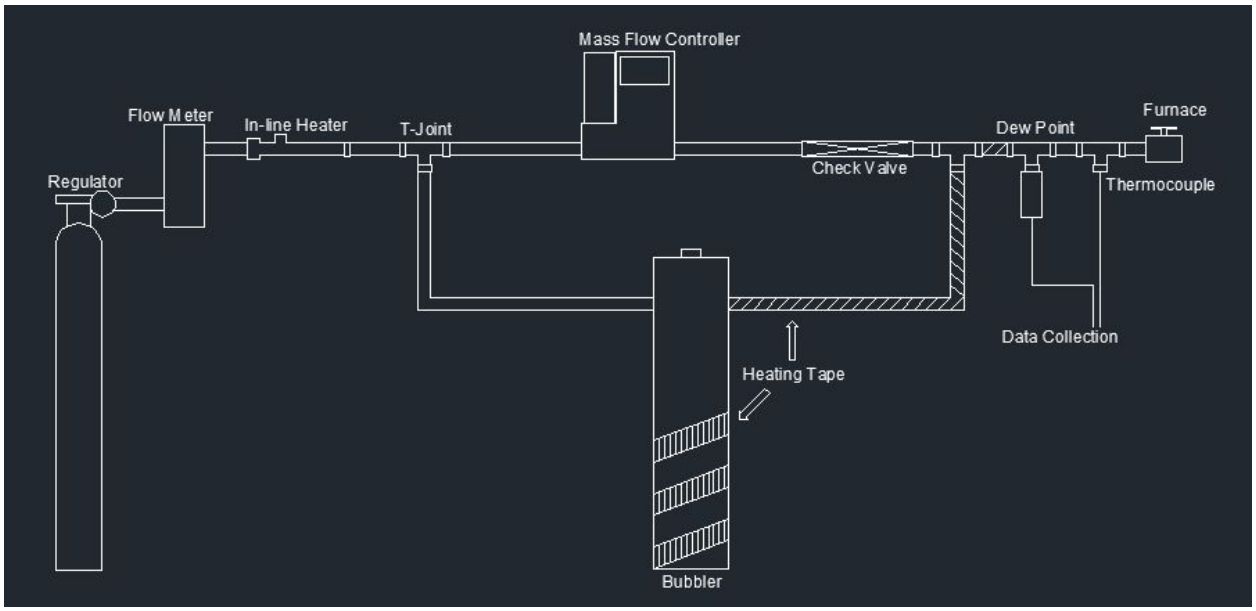

***Figure** 7-.Diagram of gas manifold to be implemented in this experiment. This design offers humidity control, and even the possibility of a humidity profile for later testing.*

III.B. Processing of Lignin Powder

The dry Kraft softwood lignin (KSL) powder goes through a series of heat treatments and processing steps for making a highly graphitic carbon composite. Thermal stabilization, pyrolysis, and reduction make up the heating steps. These steps collectively are commonly

referred to as carbonization. For this experiment, thermal stabilization is combined as a pre-step during pyrolysis in order to reduce processing time. KSL powder is contained within a ceramic crucible in a tube furnace (Thermo Scientific Lindberg Blue M model) with inert gas conditions. A detailed diagram of the furnace and the processing method can be seen in Figure 8. The thermal stabilization step results in carbon cross-linking to prevent carbon burn-off at higher temperatures. Carbon content in the powder increases during pyrolysis as organic compounds are burned. Finally, reduction stabilizes the material with the introduction of hydrogen.

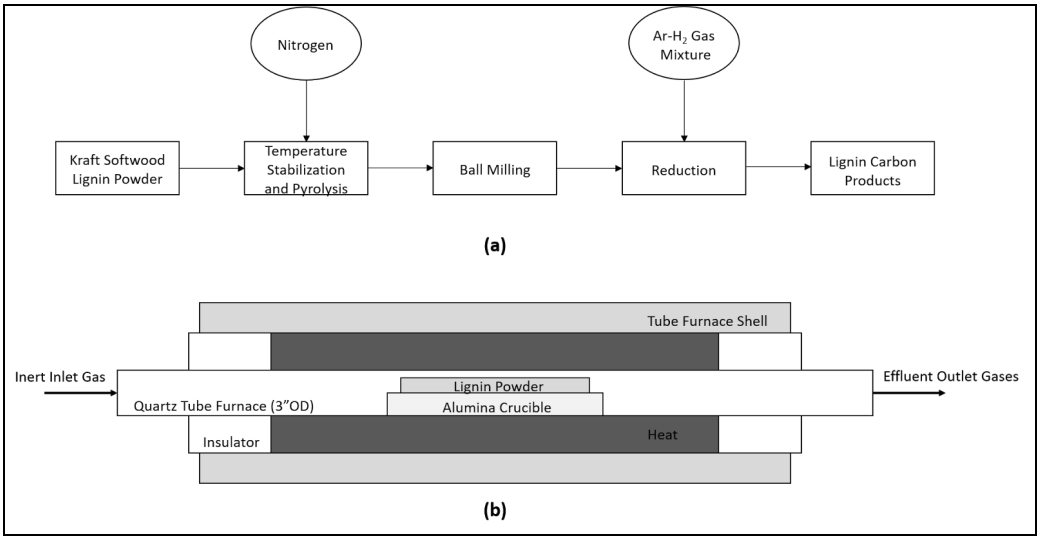

Figure 8- *Step by step process of crystallizing lignin (a) Diagram of tube furnace used in CRC (b) [15]*

KSL powder is first heated in a tube furnace for thermal stabilization and pyrolysis in a nitrogen and water vapor atmosphere. The inlet gas, N_2, passes through an H_2O bubbler and mixes with a controlled amount of dry N_2. The humidity is altered by adjusting the amount of mass flow through the dry and wet lines, as well as adjusting the heating elements. These are monitored via the dew point sensor and thermocouple mounted at the outlet of the manifold. The gas mixture enters the furnace at volumetric flow rate of 3 L min^{-1}.

The crucible is heated from 30 to 1000 °C at a rate of 10 °C min^{-1} and then held at 1000 °C for one hour. Thermochemical decomposition of the organic material starts after reaching 200 °C. The effluent gases, which include steam, nitric oxide (NO), carbon monoxide (CO), carbon dioxide (CO_2) and sulfur oxides (SO_x), leave the system and are trapped in oil. After pyrolysis, the charred powder is ground up using a two-step process in order to increase surface area and improve resulting structure. The char is initially ground using a mortar and pestle; then, the material is milled with a planetary ball mill (PM100 RETSCH model,) which results in particle sizes in the micrometer range. 2 and 10 mm stainless-steel milling media within a stainless-steel container are used in the milling process. One-third of the container is filled with sample material and ground at 350 revolutions per minute for three hours, composed of alternating 15-minute periods of milling and holds at room temperature for cooling. The material is sieved to remove the milling media. Reduction of the carbon composite is conducted at 1050 °C with a heating rate of 10 °C min^{-1} and one hour hold in an argon-hydrogen (4 % H_2) gas mixture (3 L min^{-1}.)

Five batches were made to obtain humidity values at 0, 18, 45, 75, and 105 g/m^3 during stabilization/pyrolysis processing step. The crucibles are weighed before and after being filled with lignin. Approximately 100 g of lignin powder is placed in each crucible. The loaded crucibles are placed at the center of the furnace tube. Two ceramic plugs are placed on either side of the crucibles in order to insulate the heat zone during pyrolysis. Once both ends of the tube furnace are sealed, the gas is turned on and allowed to flow through the furnace for a minute before turning the furnace on. The furnace is pre-programmed with the heating cycle, and once

started, must be checked on several times throughout the run to look for any problems. The programmed heating cycle is shown in Table 1.

Table 1- *Programmed heating cycle for pyrolysis step*

Stabilization/Pyrolysis		
Step #	Temp (℃)	Time (min)
1	30	10
2	1000	97
3	1000	60
End	30	Off

III.C. Characterization

III.C.i. X-Ray Powder Diffraction

X-ray diffraction (XRD) scans are performed at room temperature using a PANalytical Empyrean diffractometer in order to determine any crystalline structure in the processed lignin carbon. Table 2 gives the scan parameters for the powder diffraction scans, and Figure 9 shows the diffractometer in Bragg-Brentano configuration.

Table 2 - *Scan parameters for the powder diffraction scans.*

Instrument	PANalytical Empyrean Diffractometer	PANalytical Empyrean Diffractometer
Sample	LaB_6	KSL Powders
Beam Type	Cu $K_{\alpha1}$ and $K_{\alpha2}$	Cu $K_{\alpha1}$ and $K_{\alpha2}$
Wavelength [Å]	1.5406 and 1.5444	1.5406 and 1.5444
Scan Range [°2θ]	25-100	15-90
Step Size [°2θ]	0.02	0.02
Temperature [K]	298	298
Pressure	Atmospheric	Atmospheric

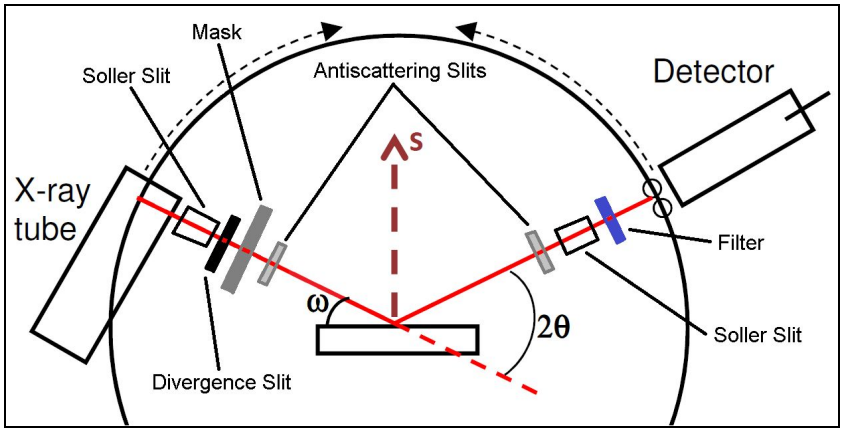

Figure 9- *Diagram of the Bragg-Brentano configuration and instrumental setup used in this experiment.*

Crystallographic planes (hkl) can be indexed for any standard pattern based on graphite with a hexagonal structure. Scanned data is refined based on peak fitting software to determine the full-width half-maximums (FWHM) of the peaks and the d-spacings. From the FWHM, one can calculate the total peak broadening. The instrumental broadening can be subtracted from the total broadening so that sample broadening can be attained. The Debye-Scherrer equation relates sample broadening and crystallite size and is given as shown [16]:

$$\tau = \frac{K\lambda}{\beta \cos\theta}$$

where τ is the mean size crystalline domain (Å), K is the dimensionless shape factor, 0.9, λ is X-ray wavelength (Å), β is line broadening at FWHM (° 2Θ), and Θ is the Bragg angle (° 2Θ). Instrumental broadening differs between diffractometers, so a calibration sample, such as NIST SRM 660c LaB_6 can be utilized to find the broadening effect of the PANalytical Empyrean. [16]

III.C.ii. Scanning Electron Microscopy

Scanning electron microscopy (SEM) allows for the evaluation of the powder morphology. Through image analysis (ImageJ), the particle sizes before and after ball milling

can also be compared. The scale of the micrograph is calibrated in the software using the scale bar given by the SEM instrument, and particles are manually measured across their length. The SEM is also equipped with an energy dispersive spectrometer (EDS) that can quickly give identification of elemental contaminants in the samples, most notably sulfur, sodium, and iron. Identification was done through point and map scans over the area of interest.

IV. RESULTS AND DISCUSSION

IV.A. Morphology and Particle Size

The carbon composite structure morphology and particle size were analyzed using SEM micrographs of each sample before and after ball-milling. Imaging of the raw lignin powder confirms powder particles on the order of 100 microns scattered and unattached, as seen in Figure 10 (A). The composite structure post-pyrolysis processing and before ball-milling shows fusion of the lignin powder into a cohesive, porous morphology caused by the carbon stabilization step, Figure 10. Larger, hollowed out pores appear to be caused by the expansion and rupturing of the individual lignin powder particles as off-gassing occurs due to decomposition. The lignin processed with water appears to have thicker pore walls and a reduced number of pores due to a higher degree of particle fusion, as seen in Figure 10. Some changes in structure with increasing pyrolysis humidity were difficult to assess; Surface area characterization, like BET analysis, could be performed to show changes in porosity and morphology after pyrolysis, ball milling, and reduction.

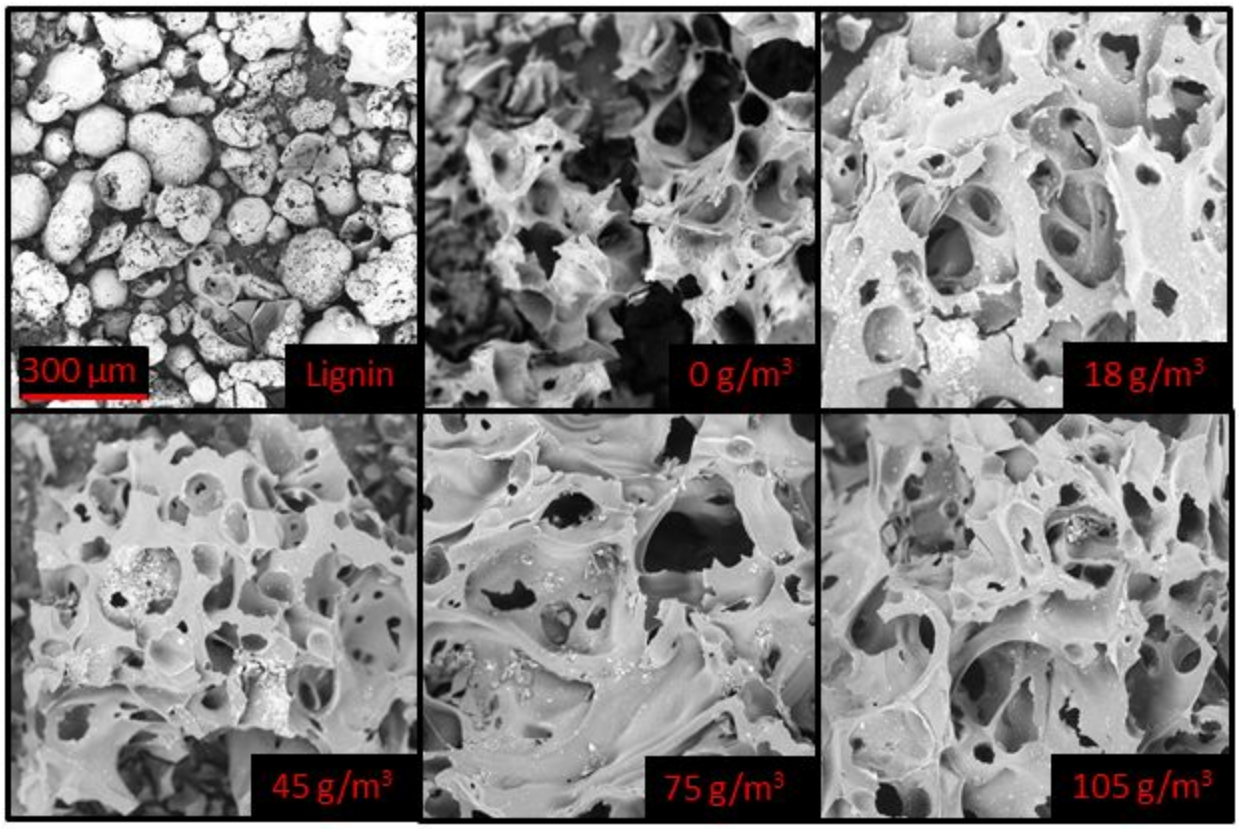

Figure 10- *SEM imaging of raw lignin and pre ball milled lignin-based carbon composites processed with water at 0 g/m³, 18 g/m³, 45 g/m³, 75 g/m³, and 105 g/m³.*

Particle size analysis was performed on the SEM images of the post-BM samples before and after the reduction step shown in Figure 11 using ImageJ image analysis software. This was done to evaluate both the effect of absolute humidity and the effect of the reduction step on the particle size. Data was gathered on a sample size of 50 randomly selected particles.

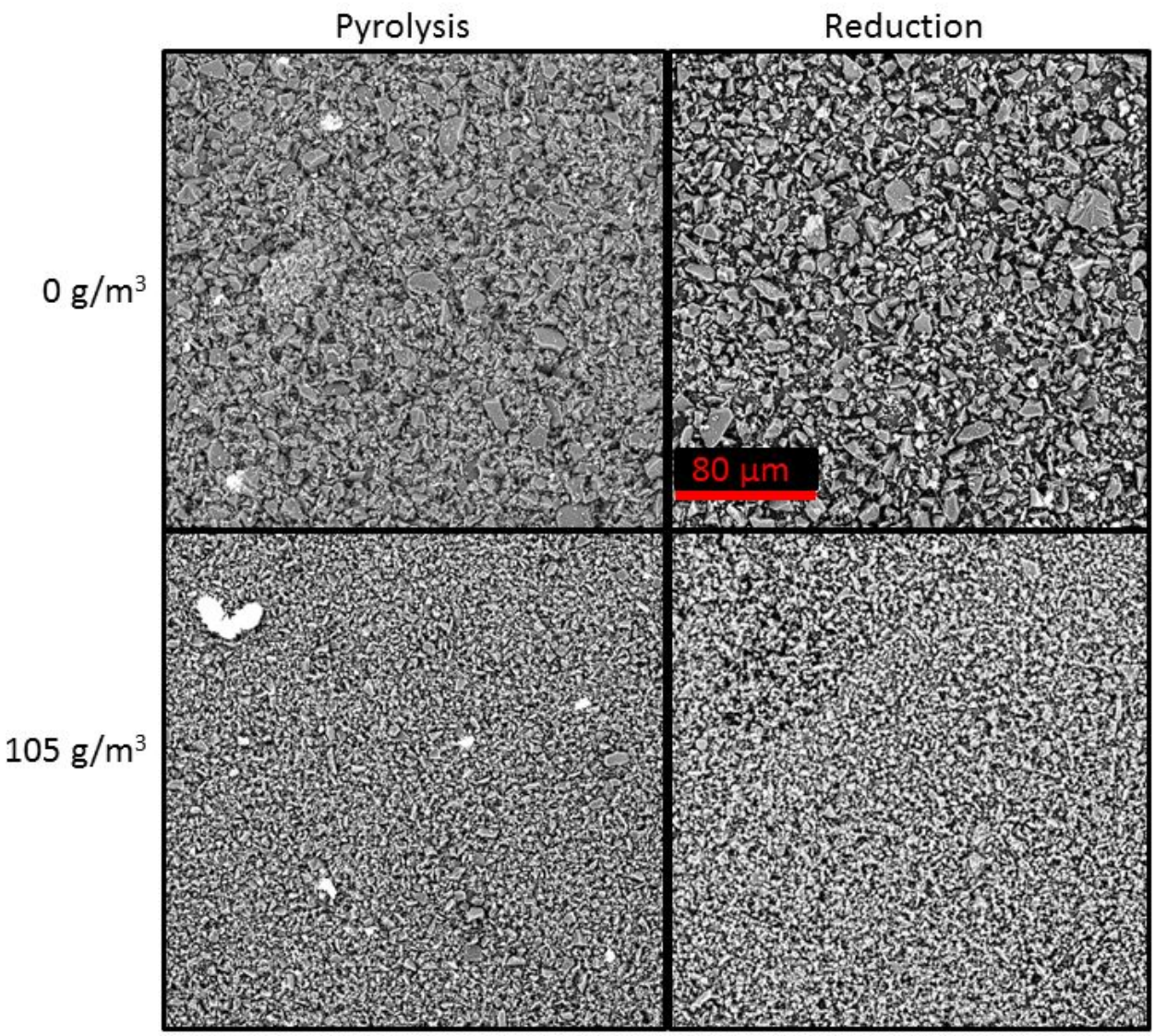

Figure 11- *SEM imaging showing the effect of increasing water in processing and of reduction on the ball-milled particle size. White contaminants are iron filings introduced during ball-milling.*

Analysis of the ball-milled pyrolyzed composite processed with no water (0 g/m^3) shows an average particle size of approximately 8 microns, versus the batch with the highest amount of water (100 g/m^3) with an average particle size of approximately 4 microns, Figure 12.

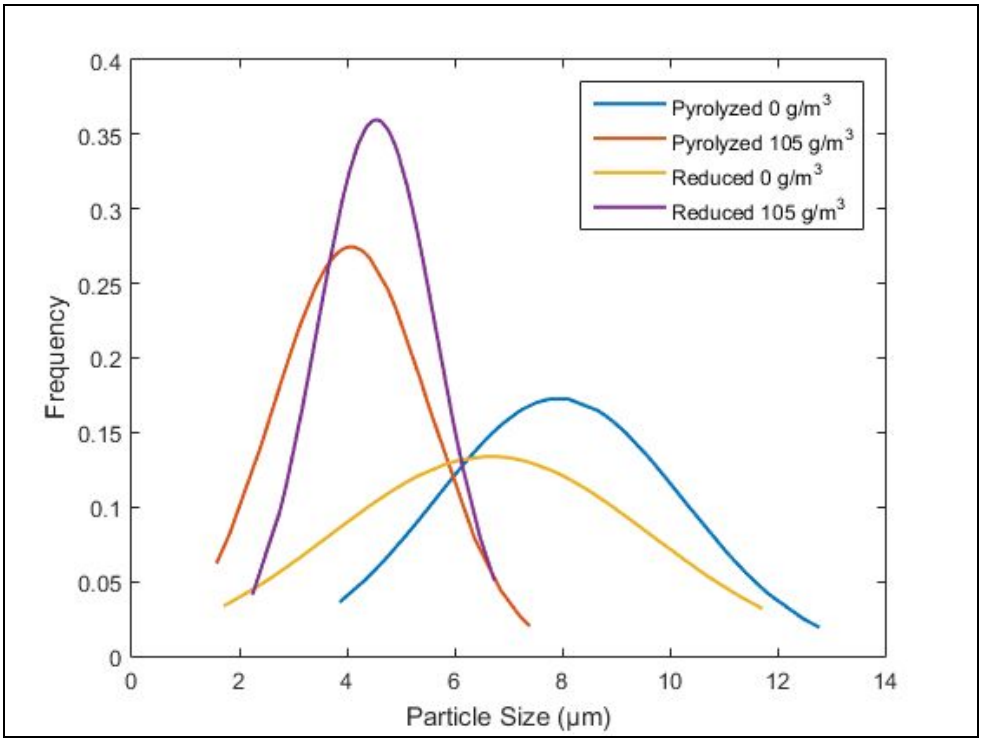

Figure 12- *Particle size distribution for the highest and lowest absolute humidity batches before and after reduction. Each distribution is made with 50 particle measurements.*

Based on the distributions, it appears that the minimum particle size for the wet- and dry-processed composites is comparable. The average size decrease in the wet batch versus the dry means that the larger particles occur more frequently in the dry batch. This indicates that the particles were easier to break up with the addition of water during processing, which suggests a reduction in mechanical properties. Although this mechanism is not fully understood, this may be caused by the increased fused structure due to water enhancing monomer mobility.

IV.B. Crystallite Size

X-ray diffraction data gives the interatomic spacing (peak position) and crystal structure (number of peaks) of our samples. As expected, the raw lignin shows no defined peaks but an amorphous curve. Figure 13 shows XRD patterns for pure graphite, raw KSL, and KSL after each processing step. Due to the small crystallite sizes of the graphitic domains, the graphite

peaks in the KSL samples appear much broader. The most visible graphite peaks in the KSL are the (002) and the (101).

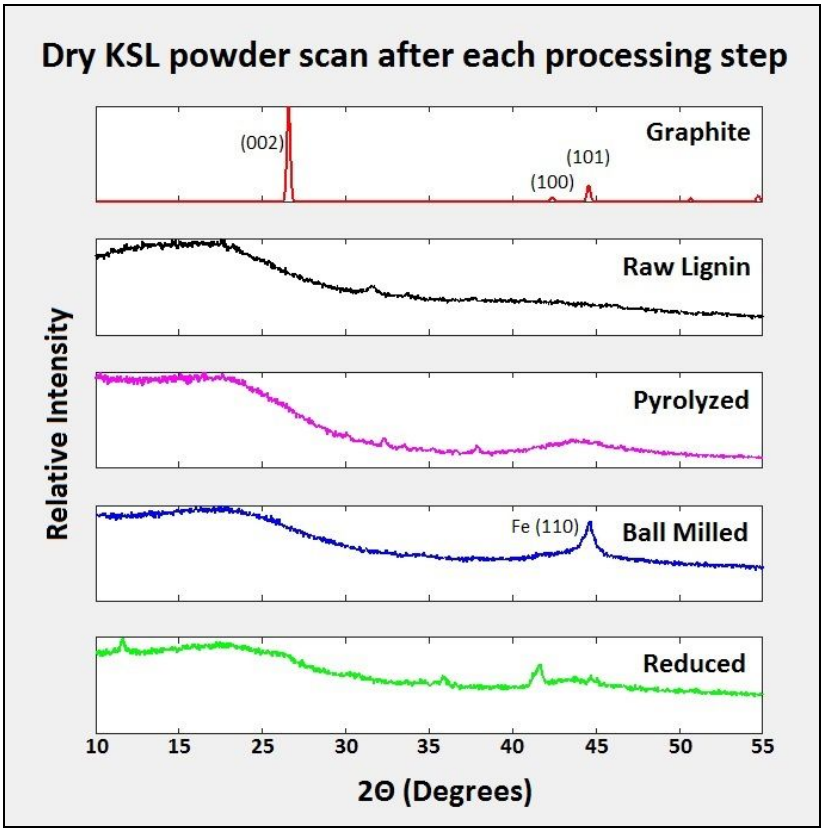

Figure 13 - *XRD patterns for pure graphite, raw KSL, and KSL after each processing step.*

The beginnings of the (002) peaks have to be differentiated from the intensity produced by the instrumental background and the amorphous carbon in order to access peak width. Post-ball milling, some samples displayed a sharp peak at roughly 44.5 °2Θ. This peak may be attributable to the BCC iron (110) peak. SEM and EDS showed iron contaminants on the micron scale. These contaminants were not present in every sample and most likely came from the stainless steel ball milling media. XRD scans were also performed for each sample from 0 to 105 g/m^3. Figure 14 shows five powder diffraction scans for each of the reduced KSL powders. Structural contaminants may obscure the graphite (101) peak on the 18 and 45 g/m^3 samples.

Contaminants could include iron, iron oxides, sulfates, sodium oxides. The graphite peak positions do not vary across the range of pyrolysis inlet gas humidities. At higher humidities, the (002) graphite peaks broaden slightly. This change in peak width can be related to graphitic crystallite size through the Scherrer equation.

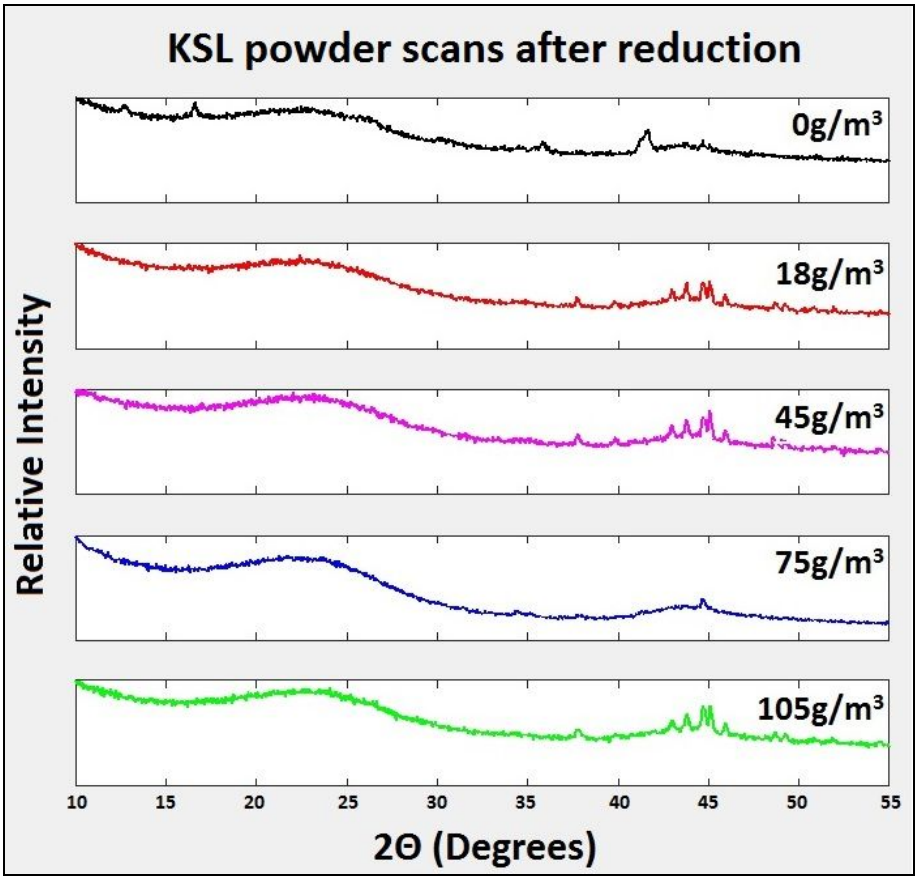

Figure 14 - *Shows five powder diffraction scans for each of the reduced KSL powders. Structural contaminants may obscure the graphite (101) peak on the 18 and 45 g / m3 samples. Contaminants could include iron, iron oxides, sulfates, sodium oxides.*

The FWHM of the (002) graphite peaks were obtained by Gaussian peaking fitting in GSAS. The goodness of fit (X^2 method) for the peak fitting of the samples (0, 18, 45, 75, and 105 g/m^3) were 1.86, 1.02, 1.16, 1.22, and 1.29 respectively. Figure 15 shows the peak fitting of the XRD scan of the reduced KSL powder in GSAS.

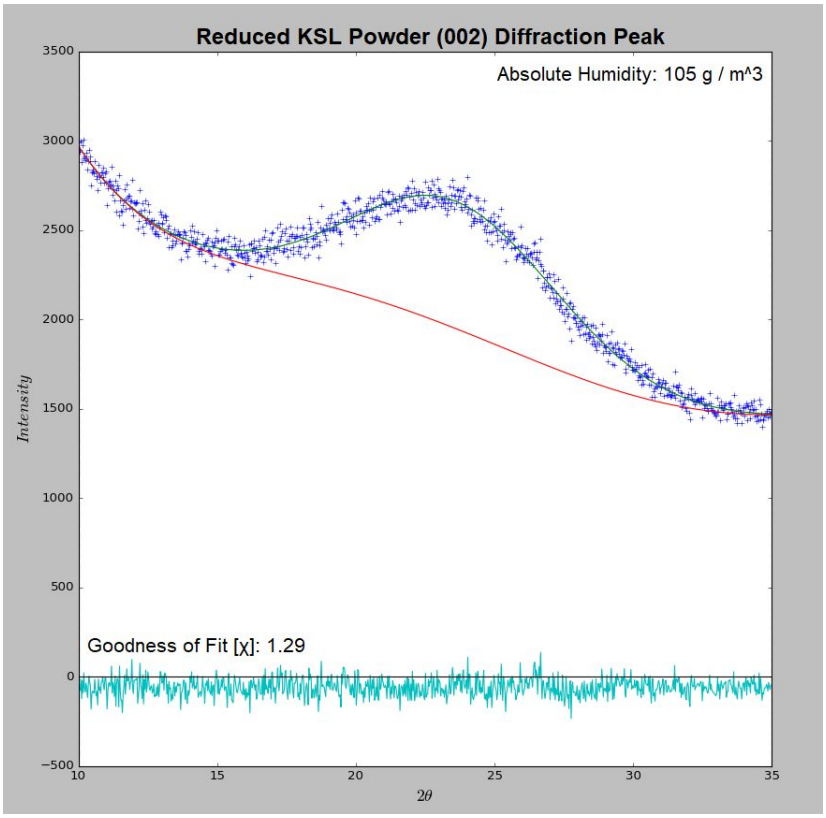

Figure 15 - *Shows the peak fitting of the xrd scan of the reduced KSL powder in GSAS.*

Using the Scherrer equation and the instrumental broadening, one can calculate the sample broadening. By analyzing the LaB_6 scan, the instrumental broadening near 24 °2Θ, the location of the graphite (002) peak, was found to be 0.0869 Δ°2Θ. The sample broadening of the reduced samples were used to calculate the crystallite sizes. Figure 16 shows the resulting crystallite sizes. Crystallite size saw a slight negative correlation with absolute humidity. We hypothesize that the small water molecules act as a plasticizer for the carbon within the KSL. While the water does not affect the growth rate of the graphitic domains, it may reducing the activation energy to create new crystallites during pyrolysis. This proposed phenomena would result more frequent and smaller graphitic domains. These crystallite sizes agree with the literature value of 8 angstroms from Garcia-Negron V., et al. [11]

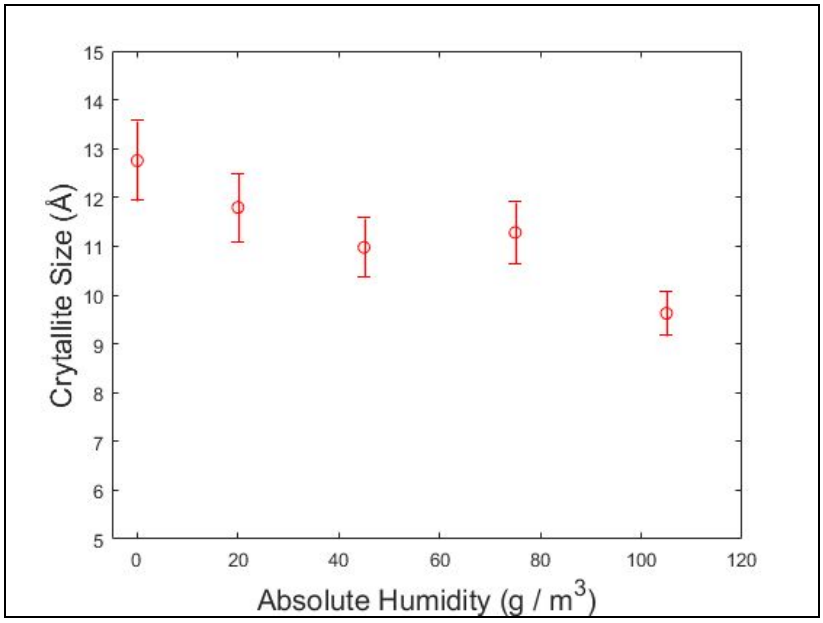

Figure 16 - *Shows the calculated crystallite sizes of the graphitic domains in the reduced KSL as a function of pyrolysis humidity. Crystallite size saw a slight negative correlation with absolute humidity.*

IV.C. Sulfur Sodium and Iron Contamination

Elemental contaminants in the graphite composite samples could negatively affect its performance as a battery anode by reducing the batteries maximum capacity or cyclic life. The three contaminants, sulfur, sodium and iron, have been quantified in a previous study, which is used for a baseline here [11]. The composite samples were observed using SEM and EDS to determine humidity's effect on contaminant content. Point and map scans were conducted on the pyrolyzed material to collect sulfur and sodium content as a function of processing humidity. The resulting data is shown in Figure 17. The processing humidity showed to have little or no effect on the sulfur and sodium content in the samples.

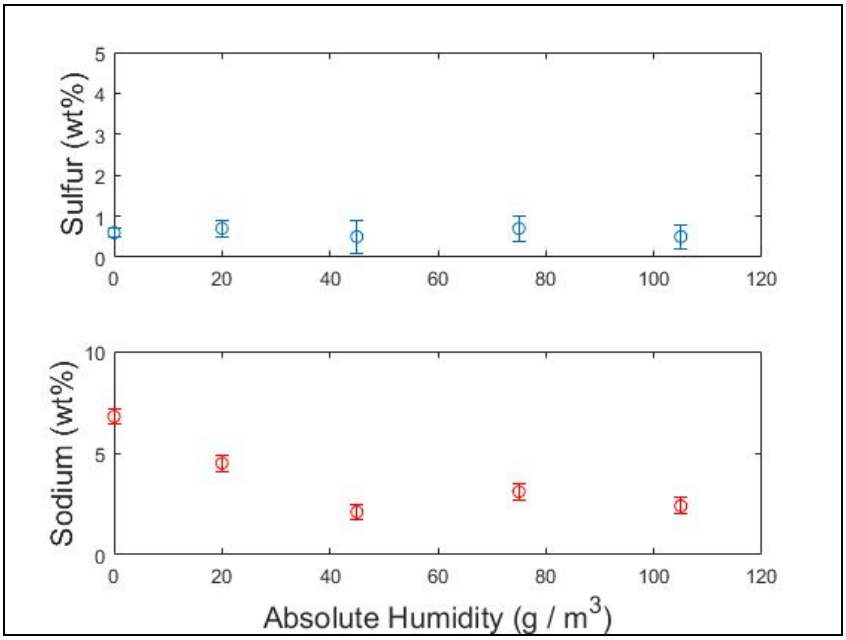

Figure 17 - *Amounts of Na and S contaminants*

Iron contaminants could not be observed using the same process because of how they were distributed in the sample. The sulfur contaminant was a byproduct of the pulping process and is evenly distributed throughout the sample while the iron contaminant is due to ball milling. The iron balls in the ball mill grind the sample to micron sized particles but in the process causes iron flakes from the balls to contaminant the sample. Due to the low iron content and large particle size relative to the composite particles, EDS could not be used to quantify iron contamination in the sample. SEM images were taken of single iron flakes shown in Figure 18 but without elemental analysis of a larger area, iron weight percent could not be calculated.

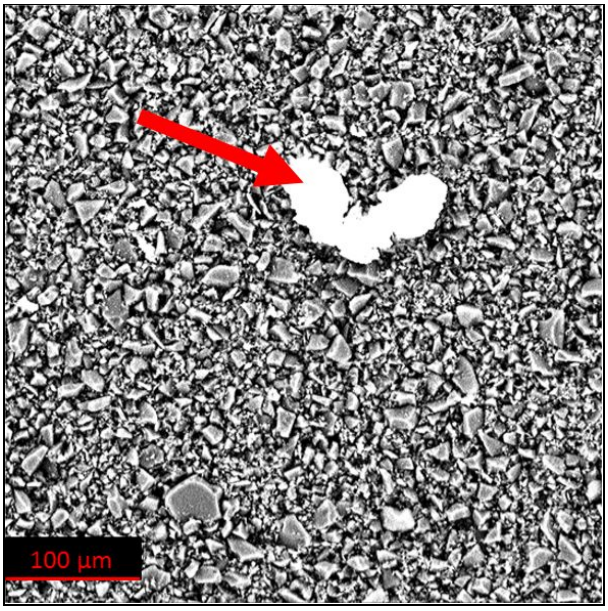

Figure 18 - *Shows iron contaminant in ball milled sample, introduced by stainless steel milling media.*

V. CONCLUSIONS

Graphite is a commonly used battery anode material because of its conductive structure. Building on previous research in processing lignin polymer waste product into a graphitic carbon composite, this investigation alters the humidity in the atmosphere during heat treatments to determine its effect on the resulting microstructure. Literature reviews were performed in order to understand the changes that occur in the lignin during the pyrolysis and reduction steps. Furthermore, the data collected during this experiment was compared to literature values from similar studies. Similar values for process yield, weight percentage of contaminants, and graphite crystallite sizes were found in this project. A gas manifold was constructed for the purpose of heating the inlet gas, as well as monitoring and controlling the humidity of the gas. The manifold was able to successfully heat the inlet gas to 60 °C, and a constant humidity within 5 g / m^3 could be maintained throughout an entire pyrolysis cycle. Analysis of the processed lignin consisted of SEM, EDS, and XRD. SEM imaging of samples post-pyrolysis showed a change in the porous

structure potentially resulting from increased mobility of the lignin monomers. X-ray diffraction measured peak broadening to determine that the crystallite size of the graphite nanoparticles after carbonization is correlates negatively with humidity. EDS, in conjunction with SEM, was used to determine the relative weight percents of the contaminates in the lignin powder.

There is future work that can be performed in several areas to further assess the graphitization process and the resulting carbon composite material. On the processing side, finding instruments that can handle higher processing temperatures and removing contaminants are key should higher water content be desired. The iron contaminant particles are large enough that it may be possible to remove them from the powder before reduction using something as simple as a magnet. The dew point transmitter cannot be run above 60 °C without losing accuracy, and the mass flow controller has a maximum operating temperature of 50 °C. The max humidity of 105 g/m^3 that was reached is close to the theoretical limit of what could be attained with our current instruments (130 g / m^3.) Furthermore, the heating elements approached their input voltage limits, meaning further heating may have been untenable. Obtaining equipment that is capable of both increasing the temperature of the gas above 60 °C and functioning properly at these increased temperatures would allow even greater humidities to be reached.

Additionally, several important facets of the carbon composite were not characterized during this experiment. The two points of interest that were not investigated were

crystallinity of the carbon composite, and an analysis of its surface area. Investigating both of these could yield valuable data on the possible performance of the composite as anode material. Researchers at the MDF will perform battery testing such as half cell galvanic cycling

and coin cell benchmarks. The data collected from the material created over the course of this experiment will aid the team at the CRC in their future research into kraft softwood lignin.

ACKNOWLEDGEMENTS

We would like to thank Dr. David Keffer and Mr. Chris Wetteland for their council as our advisors this semester, as well as Dr. David Harper and Ms. Valerie Garcìa-Negròn for sponsoring the project. Ms. Garcìa-Negròn taught us the initial processing steps and assisted in conducting experiments at the CRC. We would like to thank Dr. Lundin for instructing MSE 489, and John Bohling, the course teaching assistant. Additionally, we thank Doug Fielden, who helped us source parts to construct our manifold. We would also like to thank Dr. Jianlin Li for touring us through the MDF and explaining the future battery testing. We would like to thank the Department of Materials Science and Engineering at the University of Tennessee for their resources, facilities, and support. We would also like to thank the Center for Renewable Carbon for their facilities. Finally, we would like to thank the Electrical Power Research Facility (EPRI) for their generous funding the project.

REFERENCES

[1] Rudolf Patt et al. "Paper and Pulp" in Ullmann's Encyclopedia of Industrial Chemistry 2002 Wiley-VCH, Weinheim

[2] Hensley, R. et al. "Battery Technology Charges Forward," McKinsey & Company, http://www.mckinsey.com/business-functions/sustainability-and-resource-productivity/our-insights/battery-technology-charges-ahead

[3] Taylor, Harold A. (2005). Graphite. Industrial Minerals and Rocks (7th ed.). Littleton, CO: AIME-Society of Mining Engineers

[4] "Graphite Statistics and Information" https://minerals.usgs.gov/minerals/pubs/commodity/graphite/

[5] McNutt, N., et al., "Interfacial Li-ion localization in hierarchical carbon anodes," *Elsevier.* (2017). 830

[6] Review Of New Source Performance Standards For Kraft Pulp Mills, EPA-450/3-83-017, U. S. Environmental Protection Agency, Research Triangle Park, NC, September 1983.

[7] Reportlinker. "Global Lignin Products Market - Segmented By Product Type, Source, Application, And Geography - Trends And Forecasts (2015-2020) - Reportlinker Review." N.p., 17 Sept. 2015. Web. 08 Feb. 2017.

[8] N. Maluf, "82. THE COST COMPONENTS OF A LITHIUM ION BATTERY," Qnovo - Technology, 12-Jan-2016. [Online]. Available: https://qnovo.com/82-the-cost-components-of-a-battery/. [Accessed: 08-Feb-2017].

[9] Cobb, Jeff. "Argonne Computer Model and Implications for the Tesla Model E." *GM-VOLT : Chevy Volt Electric Car Site*. N.p., 18 Nov. 2013. Web. 08 Feb. 2017.

[10] Hubbe, Martin. "Mini-Encyclopedia of Papermaking Wet-End Chemistry." *ncsu.edu*.

[11] Garcìa-Negròn, V., et al. "Processing-Structure-Property Relationships for Lignin-based Carbonaceous Materials used in Energy Storage Applications," Energy Technol. 10.1002

[12] Hakkila, P. (1989). *Utilisation of Residual Forest Biomass*. Berlin, Springer-Verlag.

[13] Tenhaeff, W., et al. "Highly Robust Lithium Ion Battery Anodes from Lignin: An Abundant, Renewable, and Low-Cost Material," Adv. Funct. Mater. 2013

[14] Whoriskey, P. "In Your Phone, In Their Air," The Washington Post, https://www.washingtonpost.com/graphics/business/batteries/graphite-mining-pollution-in-china/

[15] McNutt, N., et al. "Structural analysis of lignin-derived carbon composite anodes," J. Appl. Cryst. (2014). 47

[16] P. Scherrer, "Bestimmung der Grösse und der inneren Struktur von Kolloidteilchen mittels Röntgenstrahlen," Nachr. Ges. Wiss. Göttingen 26 (1918) pp 98-100.

APPENDIX

Standard Operating Procedure: Wet-Dry Gas Manifold for Thermo Fisher Scientific Lindberg Blue Tube Furnace

Created: April 24, 2017

Potential Hazards

- High Temperature
- Electrical Shock
- Compressed Gases
- Flammable Materials

Personal Protective Equipment Required

- Safety Glasses
- Gloves – Temperature Resistant & Nitrile

Equipment Operating Range

- Mass Flow Controller: Temperature of gas through the controller should not exceed **50°C**. Operating flow rate range between 0 and 5 L/m.
- Dew Point Sensor: Operating temperature range between **-40°C and 85°C**. Flow rate should be between 1 and 5 L/m for best results. NOTE: Dew point sensing range between **-40°C and 60°C**.
- Custom Bubbler: Depending on volume of water in the bubbler, flow rate should not exceed 5 L/m. High flow rate may drive liquid water through the system.
- Heating Tape: Operating voltage between **0 V and 45 V**.
- In-Line Heater: Operating voltage between **0 V and 120 V**.

Using the Mass Flow Controller

1. Current flow rate is shown in the center of the display. Set Point is shown in the top right.
2. Press top right button to change set point. Use “Up” and “Down” buttons to change values, use “Select Digit” button to change value position. Press “Set” when you are done.
3. Press bottom right button to go to Select Menu then press bottom left button to go to Gas Select. Use the “Up”, “Down” and “Select” buttons to choose which gas is being used in the system.
4. NOTE: Steps 2 and 3 only need to be repeated when the selection changes, not on instrument startup.

Using the Dew Point Sensor

1. Power should be supplied by 12V adaptor wired to the sensor.
2. Sensor is read as current via a multimeter. High side (+) through green wire, low side (-) through brown wire.
3. Output current range is between 4mA and 20mA. This scales linearly to a dew point range of -40°C to 60°C.

Using the Gas Manifold

1. Open flow meter to 5 L/m or less.
2. Open inlet and outlet valves to the tube furnace.

3. Set mass flow controller set point to 5 L/m.
4. Close valve to bubbler.
5. Open gas line.
6. Adjust flow meter to desired flow rate. Check that the flow rate is the same with what the mass flow controller reads.
7. Turn on power supply to heating tape and in-line heater. NOTE: Do not turn on in-line heater without gas flow. This could damage the equipment.
8. Adjust the valve to the bubbler to change flow rate through the bubbler. Flow rate through the bubbler is the difference between flow meter and the mass flow controller. NOTE: It might be necessary to lower the mass flow controller set point to achieve higher flow rate through the bubbler.
9. Adjust voltage from the power supply to the heating elements to change inlet gas temperature.
10. Use steps 8 and 9 to achieve desired dew point.